NON-UNIQUENESS OF GEOTHERMAL NATURAL-STATE SIMULATIONS

Elvar K. Bjarkason[1,2], Angus Yeh[1], John P. O'Sullivan[1], Adrian Croucher[1] and Michael J. O'Sullivan[1]

[1]Department of Engineering Science, University of Auckland, Auckland, New Zealand

[2]Institute of Fluid Science, Tohoku University, Sendai, Japan

e.bjarkason@tohoku.ac.jp

Keywords: *Natural state, steady state, uniqueness, convergence, reservoir modelling, TOUGH2.*

ABSTRACT

A numerical simulation representing the natural state of a geothermal system commonly involves finding an approximate solution to a mass and energy balance equilibrium problem; that is, solving a steady-state simulation. Solving this type of natural-state simulation problem is often problematic, and geothermal simulators regularly struggle or are unable to achieve a reasonable steady-state solution for a given geothermal model. When a simulator achieves a steady natural state, it is usually assumed that the simulated natural state is unique for the chosen model parameters. However, as we show here, this uniqueness assumption may be wrong as there might be multiple equilibrium solutions for a single natural-state model. Using a model based on a working model of the Wairakei-Tauhara geothermal field, we demonstrate how multiple equilibrium or steady-state solutions can be achieved for a fixed set of rock properties and model boundary conditions. The different steady-state solutions are found by varying the initial conditions used to initialize the transient to steady-state simulations which model the natural state. For the presented example, we were able to find four different steady-state solutions to a natural-state problem. Although the large-scale temperature distributions are similar, these four simulated natural states have temperatures which, in parts of the model, differ by up to 122°C: a model discrepancy which is substantially greater than expected temperature observation errors. This uniqueness problem, therefore, complicates natural-state model inversion or calibration.

1. INTRODUCTION

Developing a model which can accurately represent the natural state of a geothermal reservoir is both challenging and time-consuming. In principle, standard natural-state computer models represent the pre-exploitation state of a geothermal system by a steady-state simulation problem, which is solved using a transient simulation run up to a large simulation time (O'Sullivan et al., 2001). These transient to steady-state simulations commonly converge slowly to a solution. Therefore, it can be problematic, in practice, to achieve an acceptable steady-state solution within a reasonable time frame. Furthermore, a steady-state solution may not necessarily exist for certain combinations of model parameters and boundary conditions. However, when a steady-state solution is achieved, it is usually assumed that the simulated natural state is unique for the chosen model parameters and boundary conditions. But uniqueness is not necessarily guaranteed for a steady-state geothermal simulation.

Here we bring attention to the issue that a simulated natural state may be non-unique even if a steady state is achieved. Some geothermal modellers may have been aware of this issue. Bodvarsson et al. (1982), for instance, questioned whether their two-dimensional (vertical slice) natural-state model describing the Krafla geothermal system had a unique steady-state solution. They checked for potential non-uniqueness of their natural-state model by rerunning their transient to steady-state simulation using a different initial condition to the one they used previously but found the same steady-state solution as before. Based on those results, they concluded that their achieved steady state might be unique. However, more nonlinear three-dimensional natural-state models may be more prone to having non-unique steady-state solutions. Non-uniqueness problems can also arise in other nonlinear subsurface models, such as groundwater models that allow for a dynamically varying water table (Reilly & Harbaugh, 2004). Nevertheless, it seems that geothermal modellers are either not aware of the problem or, as the present authors have mostly done in the past, overlook the non-uniqueness issue.

To illustrate the fact that a simulated natural state can be non-unique, we use a three-dimensional model based on a working model used to describe the Wairakei-Tauhara geothermal system. For a natural-state model with fixed model parameters and boundary conditions, we were able to generate four different steady-state solutions (see, e.g., Figure 7). These different natural states were generated by using different initial conditions to initialize the transient to steady-state simulations. As shown in Figure 3, simulated natural-state temperatures differed by up to 122°C, which is a considerable model discrepancy. Therefore, this non-uniqueness issue is problematic when the goal is to invert or calibrate a natural-state model, as discussed in the following section. This issue raises questions about how best to model and invert the natural state of a geothermal system. Although we do not present a framework here to address this uniqueness problem, we suggest that a standard natural-state inversion workflow should at least include some attempts to check whether a calibrated natural-state model has a non-unique steady state.

2. GENERATING THE DIFFERENT NATURAL STATES

2.1 The Numerical Reservoir Model

For the simulation results presented here, the reservoir simulator we used was AUTOUGH2 (Yeh et al., 2012), which is The University of Auckland's version of the widely used TOUGH2 simulator (Pruess et al., 1999; Pruess, 2004). The model we consider is based on a natural-state model of the Wairakei-Tauhara geothermal system. The model is similar to the Wairakei-Tauhara model presented by Yeh et al. (2016).

The Wairakei-Tauhara like model used here is a pure water model which has wet atmospheric boundary conditions. The model has a 34 km by 30 km rectangular footprint in the

horizontal plane, and the elevation of the top of the model is varied to approximately follow water-table levels observed in Wairakei-Tauhara. All model blocks are regular rectangular boxes with a 1 km by 1 km base, but they vary in height depending on which model layer they are in. In total, the model has 39,896 blocks and 56 layers.

Large volume blocks (with a volume of 10^{50} m^3 each) are used to prescribe constant (top boundary) temperature and pressure conditions at the top of each column in the model. The side boundaries of the model are closed. The base of the model includes a mixture of heat-flux and mass-flux boundary conditions.

2.2 Creating Different INCON Files and Natural States through Inversion

As part of an ongoing effort to improve inversion methods used for geothermal reservoir modelling, we considered the Wairakei-based model as a synthetic inversion test case. Using this model, we wanted to test and demonstrate how adjoint-based inversion algorithms (see, e.g., Bjarkason et al. (2018, 2019)) may speed-up inversion of realistic three-dimensional geothermal reservoir models. As expected (see Bjarkason et al. (2018)), we found that the cost of applying adjoint and direct methods, to generate model sensitivities or derivatives to guide inversions of the Wairakei-based natural-state model, was insignificant in comparison to the cost of nonlinear natural-state simulations.

Using the Wairakei model, we generated synthetic natural-state data by running a steady-state simulation for selected model parameters and boundary conditions. The natural-state data consisted of 1,129 temperature observations taken down selected wells. We also added Gaussian noise with zero mean and a standard deviation of 0.5°C to the data to simulate observation noise. As an initial baseline or sanity check, we looked at using the synthetic data for estimating or inverting the vertical permeability and the two horizontal permeabilities of a single rock-type in the model, while keeping all boundary conditions and other model parameters the same as those in the model used to generate the data. Even though there were only three adjustable model parameters for this inversion experiment, we used a randomized (2-view) Levenberg-Marquardt inversion algorithm proposed by Bjarkason et al. (2018) as the inversion method. This inversion algorithm uses adjoint and direct code to facilitate efficient inversion of highly-parameterized geothermal models.

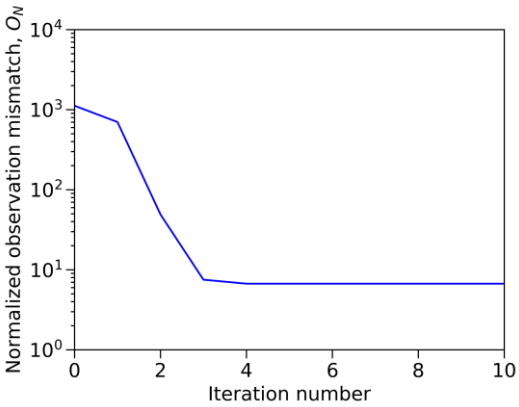

Figure 1: Convergence of the normalized observation mismatch during iterative inversion.

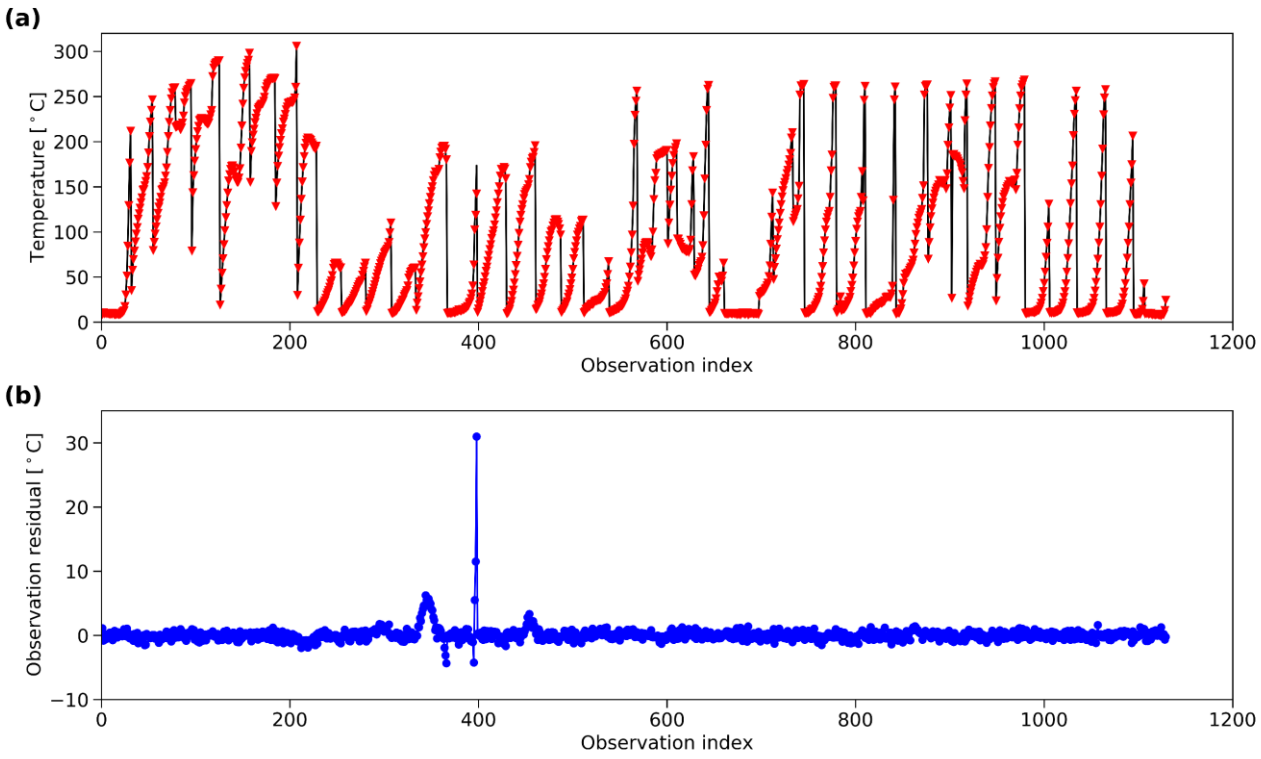

Figure 2: Inversion results. (a) Matched temperature profiles (solid black line) and temperature observations (red triangles). (b) Residual differences between the inverted temperatures and the temperature observations.

Figure 1 shows the convergence of the so-called normalized observation mismatch during the iterative inversion of the natural-state model. The normalized observation mismatch is defined as $O_N = O_d / N_d$, where N_d is the number of observations and O_d is a scaled sum of squared differences between the observations and the simulated observations. The scaling factor is given by the inverse of the variance of the observation noise. For the true model parameters and any model that gives observation matches that are consistent with the observation noise, the value of O_N should be close to unity. The adjoint-based inversion algorithm was successful at reducing O_N substantially below the initial value; however, the inverted model gave a normalized observation mismatch which had a value which was close to an order of magnitude greater than what we expected (see Figure 1). As will become clear later, the issue was not the performance of the inversion algorithm but instead the fact that the steady-state solution for the true reference model used to generate the data was not unique.

Inspecting the observation matches given by the inverted model, Figure 2 shows that most of the observations were matched within the level of measurement noise. Notably, however, there was a badly matched well with an observation residual error above 30°C (see Figure 2(b)), which is well beyond the level of observation noise. This was an unexpected result since the estimated model parameters were close to the true ones.

The reason for this significant model mismatch was that the steady state was non-unique and the simulated natural state depended on the initial conditions used to initialized the transient to steady-state simulation using the true reference parameters. In TOUGH2, the initial conditions are specified by a so-called INCON file. As is commonly done in practice, we updated the latest INCON file during inversion based on the simulated natural state of the most recent model update. At the end of the inversion, this gave an INCON file which was different from the one used for generating the data. Here we call the final INCON file generated at the end of the inversion process INCON2, and we use INCON1 to denote the INCON file used to generate the synthetic data.

Running the true reference model using INCON2 gave temperature profiles and residuals that looked nearly identical to the ones shown in Figure 2 for the inverted observation matches. The suboptimal matches were, therefore, not related to the inversion converging to a suboptimal set of model parameters. Instead, the issue was that, for fixed model parameters, the steady-state solution was not unique and depended on the chosen INCON file. This is problematic for standard inversion methods, which assume that a model using fixed model parameters consistently gives the same model outputs.

Running the same type of inversions using different adjustable parameters, we were able to generate two more INCON files, which resulted in another set of different steady-state solutions when using the true reference parameters. We call these INCON files INCON3 and INCON4.

2.3 Comparing the Different Steady States

Figure 3 compares the differences between simulated natural-state block temperatures and pressures when using the four different INCON files to initialize natural-state simulations using the true reference model parameters. Simulated block pressures disagreed by up to about 2 bar. The largest temperature differences between the natural states found using INCON1 and INCON2 are about 60°C. The temperature differences between the INCON1 derived natural state and the INCON3 or INCON4 results are even greater, with natural-state temperatures disagreeing by up to 122°C. These temperature differences are considerably greater than what we would consider reasonable for measurement errors.

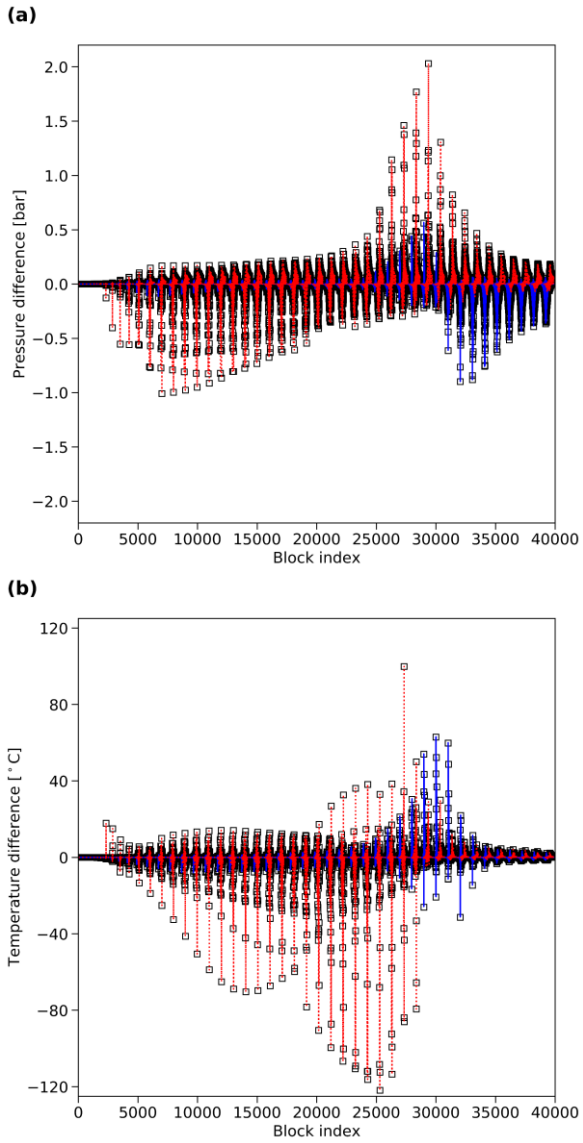

Figure 3: Differences between simulated natural-state block (a) pressures and (b) temperatures found using different initial condition (INCON) files. Shown are differences between the natural-state values found using INCON1 and the natural-state values found using INCON2 (solid blue lines), INCON3 (red dotted lines) and INCON4 (black squares).

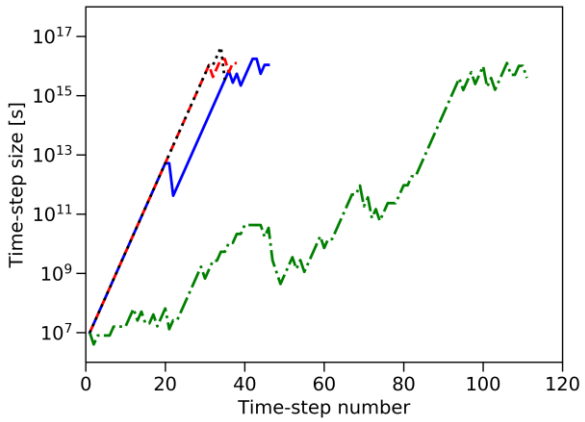

Figure 4: Evolution of time-step increments for four natural-state simulations using different initial condition (INCON) files: INCON1 (solid blue line), INCON2 (dashed red line), INCON3 (dash-dotted green line), and INCON4 (black dotted line).

For the simulation results presented here, we ran all transient to steady-state simulations up to a final time of 10^{17} s. Figure 4 shows that, for all four natural-state simulations, the simulator reached a large final time-step, which suggests that the simulator achieved an equilibrated natural state in all four cases. To check whether the simulated steady states had equilibrated, we repeated the same simulations using tighter convergence tolerances. Those simulations were consistent with the results shown here. Additionally, we solved the same steady-state problems using the TOUGH2 simulator available in iTOUGH2 (Finsterle, 2007; Finsterle & Pruess, 1995), and the recently developed TOUGH3 (Jung et al., 2017) and Waiwera (Croucher et al., 2017, 2018) simulators. All three simulators gave results consistent with those found using AUTOUGH2. This suggests that the four different natural-state solutions we achieved can be considered as adequate numerical steady-state solutions.

Figure 5 shows how the block temperatures changed from the initial temperatures specified by each INCON file to the final simulated natural-state temperatures. The natural states found using INCON2 and INCON4 are nearly identical to the specified initial conditions (see Figures 5(b) and (d)). This is reflected in the rapid time-step increase when using INCON2 and INCON4 (see Figure 4). However, for the simulations using INCON1 and INCON3, the initial conditions were relatively far from the respective natural states (see Figures 5(a) and (c)) and the simulations, therefore, converged more slowly (see Figure 4).

Comparing the INCON1 file with INCON2 and INCON4 we see that the major temperature differences that appear in the respective natural states already appear in those INCON files (see Figure 6). However, we did not make the same observation when comparing INCON3 with the other INCON files since the initial conditions specified by INCON3 are far away from the resulting natural state.

Further comparisons are made in Figures 7 and 8 between the temperature distributions given by the four steady-state solutions. In both figures, the northern end of the model is towards the top of each figure, and the western end of the model is towards the left side. Figures 7 and 8 compare steady-state temperatures in model layers 41 and 46, which gave the largest temperature discrepancies between the simulated steady states. Note that Figures 7 and 8 do not show the full range of temperatures in each layer since the temperature plots were truncated to show the main differences more clearly.

Figures 7 and 8 show that the larges temperature differences appear in the north-west end of the Wairakei convection plume and the southern end of the Tauhara convection plume. As Figure 7 shows for layer 41, the natural states using INCON3 and INCON4 include a hot convection cell towards the north-west end of the model that extends further out than is the case when using INCON1 and INCON2. In layer 46, the largest temperature differences appear towards the southern end of the model (see Figure 8). There the high-temperature plume extends further when using INCON1 and INCON3 than is the case when using INCON2 and INCON4. The same features can be seen when comparing the mass flow rates through the tops of layers 41 and 46 (see Figures 9 and 10).

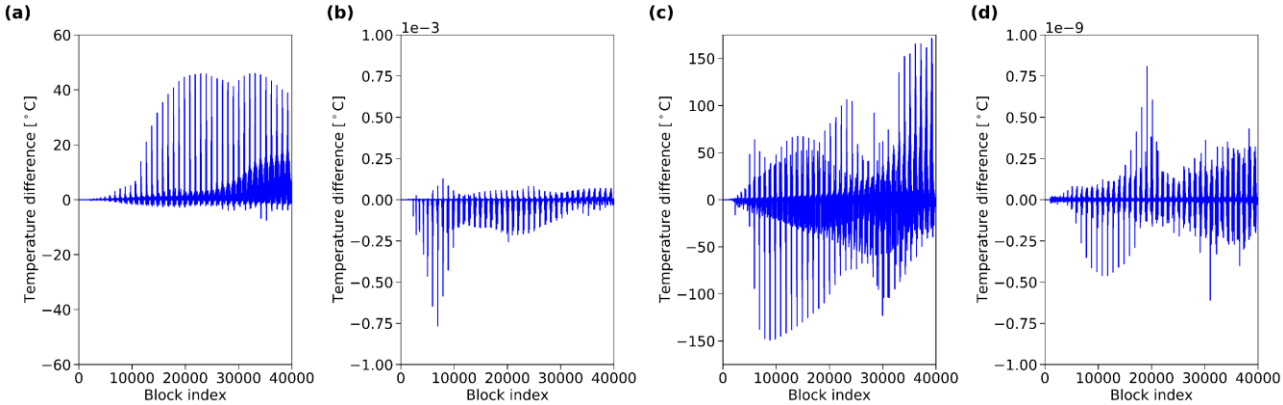

Figure 5: Differences between simulated natural-state block temperatures and block temperatures given by the initial condition (INCON) file when using (a) INCON1, (b) INCON2, (c) INCON3 and (d) INCON4.

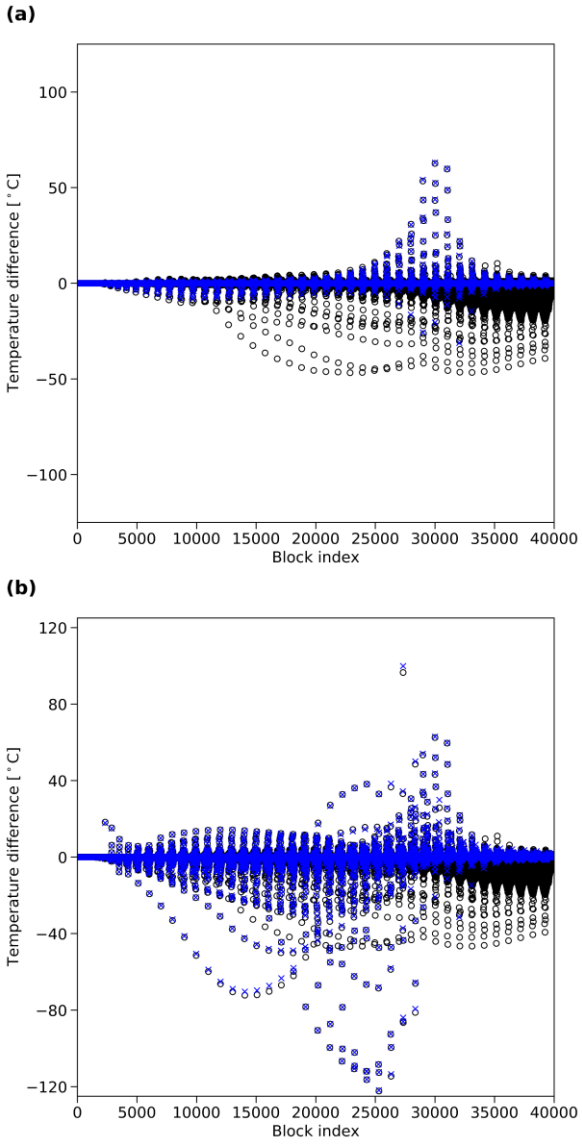

Figure 6: (a) Differences between block temperatures specified by INCON1 and INCON2 (black circles) and differences between simulated natural-state temperatures found using INCON1 and INCON2 (blue crosses). (b) Same comparison between INCON1 and INCON4.

3. WHAT CAUSES THE NON-UNIQUENESS?

At the time of writing this paper, we have not managed to identify the source of non-uniqueness for the steady-state simulation problem discussed above. As mentioned in Section 2.3, the results suggest that the four different solutions we achieved to the same steady-state simulation problem had adequately converged to an equilibrated steady-state solution. Therefore, we do not suspect that the observed non-uniqueness was caused by a lack of convergence of the numerical reservoir simulator.

Based on a suggestion given by an anonymous reviewer we considered whether the non-uniqueness could be related to residual saturation regions defined in the relative permeability curves we used, where one of the fluid phases is immobile for a range of saturation values. However, the liquid and vapour phases were both always mobile in all the two-phase zones present in the simulated natural states—we used relative permeability curves with a residual liquid saturation of 0.7 and a residual vapour saturation of 0, and all four steady-state solutions had vapour saturations below 0.2 in the two-phase regions. Therefore, the non-uniqueness is not related to the residual saturation regions.

Currently, we can only speculate about what may explain the non-uniqueness. For instance, it might be the case that the numerical heat and mass transport equations being solved fundamentally allow for multiple steady-state solutions which have dissimilar convection cells. Though it would be useful to be able to identify the source of non-uniqueness, for now, we want to bring attention to this non-uniqueness issue.

4. DISCUSSION AND CONCLUSIONS

The above results demonstrate that a steady-state model used to describe the natural state of a convective geothermal system may have multiple steady-state solutions for a fixed choice of model parameters and boundary conditions. This non-uniqueness issue arose while we were conducting an inversion experiment on a three-dimensional, synthetic natural-state or steady-state model where the task was to use synthetic observations to estimate the permeabilities of a formation. Since the true model used to generate the synthetic observations had a non-unique steady-state solution, using the same model parameters as the true model did not necessarily result in simulated observations which were consistent with the synthetic observations. Furthermore, the differences between the simulated observations and synthetic observations were not necessarily insignificant and could be as high as 120°C for natural-state temperature observations. Therefore, natural-state uniqueness issues were shown to be problematic for the synthetic inverse problem considered in this study. We expect that non-unique natural-state solutions may also arise and be problematic when dealing with natural-state models describing real fields.

This raises the question of whether a steady-state simulation approach is the most suitable tool for characterizing geothermal natural states. Considering that steady-state geothermal simulations may have non-unique solutions and that geothermal reservoirs are dynamic systems which naturally vary with time (see, e.g., Gunnarsson & Aradóttir (2015)), it might be more appropriate to formulate the natural-state problem as a state estimation problem where the adjustable model parameters are the simulation state variables (e.g., block pressures and temperatures) which are used to initialize production simulations. A state estimation approach would not require the natural or pre-exploitation simulation state variables to be at steady state, which is unlike the current standard natural-state modelling approach which involves estimating rock properties (e.g., permeabilities) and boundary conditions for a steady-state model describing the pre-exploitation conditions of a geothermal system. However, formulating the natural-state problem as a state estimation problem raises other challenges such as how to ensure that estimated natural-state or pre-exploitation conditions are physically plausible.

For the current industry-standard approach of applying steady-state simulations to describe geothermal natural states, it is at least advisable to rerun steady-state simulations for a calibrated natural-state model using multiple different initial conditions to check for potential non-uniqueness. Non-uniqueness of steady-state models adds an additional layer of model uncertainty in the geothermal context and it can be considered as a form of model error. Therefore, there is an even greater reason to consider using uncertainty

quantification algorithms which can account for model uncertainty and model error when dealing with natural-state geothermal models. Since quantifying model uncertainty typically involves generating multiple models which approximately match available observations, uncertainty quantification algorithms may potentially be suited to dealing with issues related to non-uniqueness of natural-state models.

ACKNOWLEDGEMENTS

The first author thanks Landsvirkjun (the National Power Company of Iceland) for partially funding this research.

REFERENCES

Bjarkason, E. K., Maclaren, O. J., O'Sullivan, J. P., & O'Sullivan, M. J. (2018) Randomized truncated SVD Levenberg-Marquardt approach to geothermal natural state and history matching. *Water Resources Research*, 54, 2376–2404.

Bjarkason, E. K., O'Sullivan, J. P., Yeh, A., & O'Sullivan, M. J. (2019) Inverse modeling of the natural state of geothermal reservoirs using adjoint and direct methods. *Geothermics*, 78, 85–100.

Bodvarsson, G. S., Pruess, K., Stefansson, V., & Eliasson, E. T. (1982) Modeling studies of the natural state of the Krafla geothermal field, Iceland. *Proceedings 8th Workshop on Geothermal Reservoir Engineering*, 211–217. Stanford University, Stanford, California.

Croucher, A., O'Sullivan, J., Yeh, A., & O'Sullivan, M. (2018) Benchmarking and experiments with Waiwera, a new geothermal simulator. *Proceedings 43rd Workshop on Geothermal Reservoir Engineering*. Stanford University, Stanford, California.

Croucher, A., O'Sullivan, M. J., O'Sullivan, J., Pogacnik, J., Yeh, A., Burnell, J., & Kissling, W. (2017) Geothermal Supermodels Project: An update on flow simulator development. *Proceedings 39th New Zealand Geothermal Workshop*. Rotorua, New Zealand.

Finsterle, S. (2007) *iTOUGH2 User's Guide, Report LBNL-40040*. Lawrence Berkeley National Laboratory, Berkeley, California.

Finsterle, S., & Pruess, K. (1995) ITOUGH2: Solving TOUGH inverse problems. *Proceedings TOUGH Workshop*, 287–292. Lawrence Berkeley National Laboratory, Berkeley, California.

Gunnarsson, G., & Aradóttir, E. S. P. (2015) The deep roots of geothermal systems in volcanic areas: Boundary conditions and heat sources in reservoir modeling. *Transport in Porous Media*, 108(1), 43–59.

Jung, Y., Pau, G. S. H., Finsterle, S., & Pollyea, R. M. (2017) TOUGH3: A new efficient version of the TOUGH suite of multiphase flow and transport simulators. *Computers & Geosciences*, 108, 2–7.

O'Sullivan, M. J., Pruess, K., & Lippmann, M. J. (2001) State of the art of geothermal reservoir simulation. *Geothermics*, 30(4), 395–429.

Pruess, K. (2004) The TOUGH codes—A family of simulation tools for multiphase flow and transport processes in permeable media. *Vadose Zone Journal*, 3, 738–746.

Pruess, K., Oldenburg, C., & Moridis, G. (1999) *TOUGH2 User's Guide, Version 2.0*. Lawrence Berkeley National Laboratory, Berkeley, California.

Reilly, T. E., & Harbaugh, A. W. (2004) *Guidelines for evaluating ground-water flow models, USGS Scientific Investigations Report 2004-5038*. U.S. Geological Survey, Reston, Virginia.

Yeh, A., Croucher, A. E., & O'Sullivan, M. J. (2012) Recent developments in the AUTOUGH2 simulator. *Proceedings TOUGH Symposium*. Lawrence Berkeley National Laboratory, Berkeley, California.

Yeh, A., O'Sullivan, M. J., Newson, J. A., & Mannington, W. I. (2016) Use of PEST for improving a computer model of Wairakei-Tauhara. *Proceedings 38th New Zealand Geothermal Workshop*. Auckland, New Zealand.

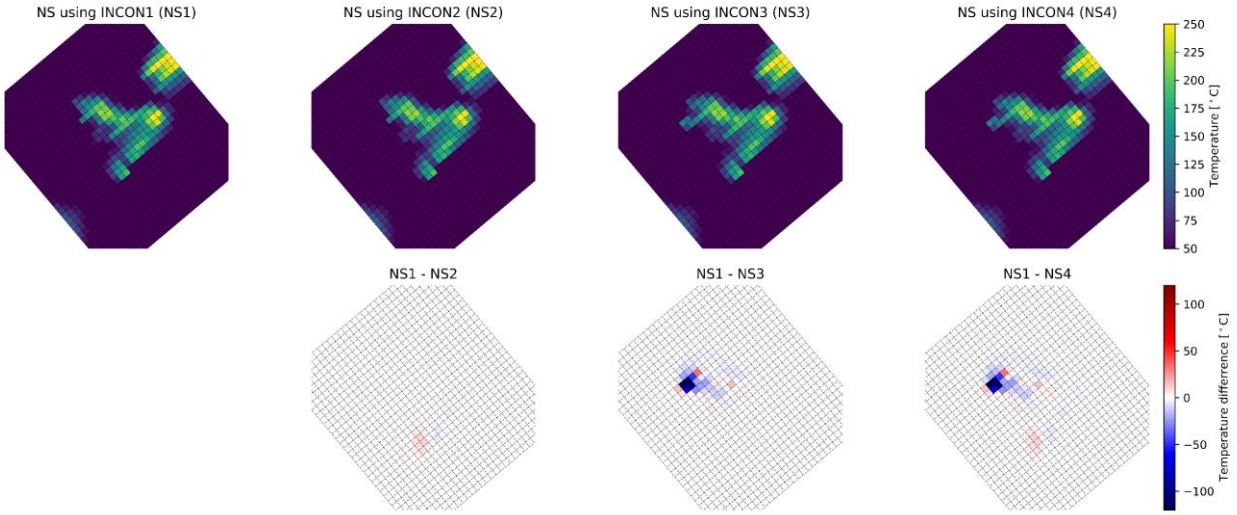

Figure 7: The top row shows simulated natural-state (NS) temperatures in layer 41 of the model when using four different initial condition (INCON) files: INCON1 (first column), INCON2 (second column), INCON3 (third column), and INCON4 (fourth column). The bottom row shows deviations from the temperatures found in layer 41 using INCON1.

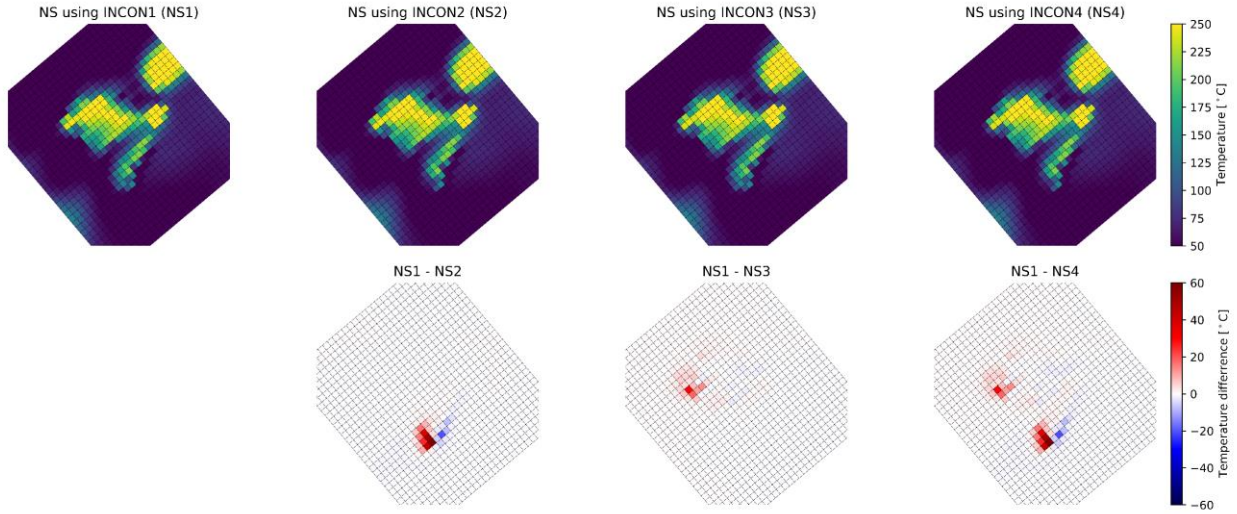

Figure 8: The top row shows simulated natural-state (NS) temperatures in layer 46 of the model when using four different initial condition (INCON) files: INCON1 (first column), INCON2 (second column), INCON3 (third column), and INCON4 (fourth column). The bottom row shows deviations from the temperatures found in layer 46 using INCON1.

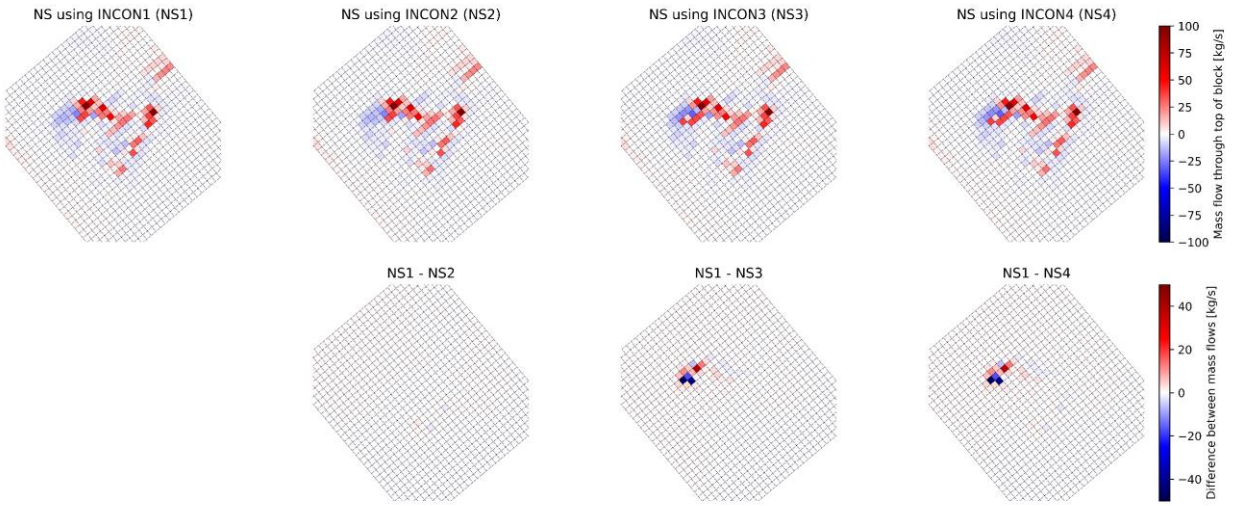

Figure 9: The top row compares mass flows through the top of layer 41 for the natural states (NS) found using four different initial condition (INCON) files: INCON1 (first column), INCON2 (second column), INCON3 (third column), and INCON4 (fourth column). The bottom row shows deviations from the mass flows found using INCON1.

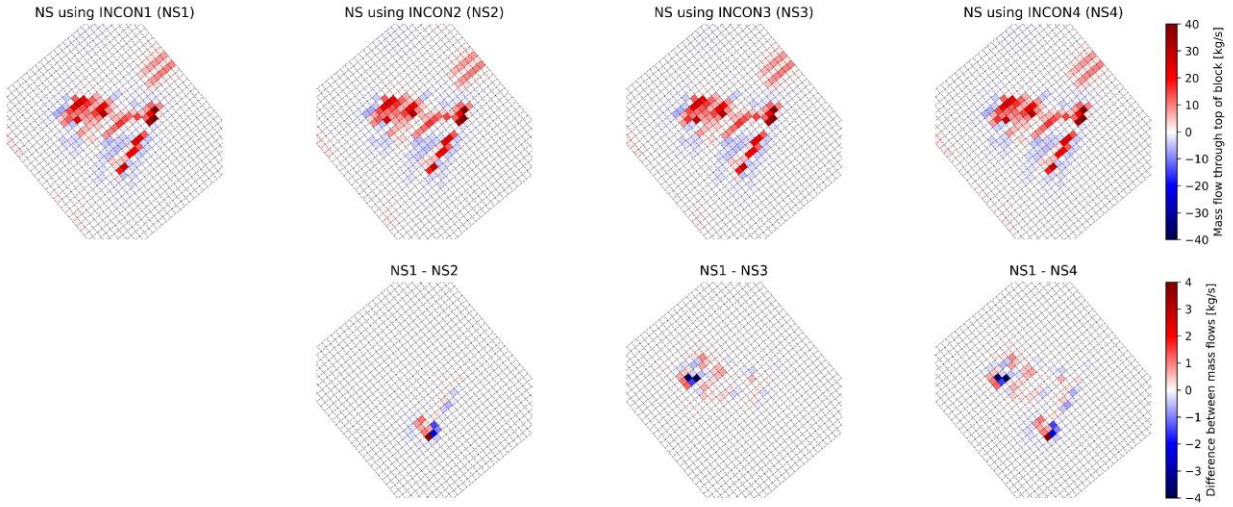

Figure 10: The top row compares mass flows through the top of layer 46 for the natural states (NS) found using four different initial condition (INCON) files: INCON1 (first column), INCON2 (second column), INCON3 (third column), and INCON4 (fourth column). The bottom row shows deviations from the mass flows found using INCON1.